

---

# Implications of H.E.S.S. observations of pulsar wind nebulae

O.C. de Jager<sup>1</sup>, A. Djannati-Atai<sup>2</sup>

<sup>1</sup> Unit for Space Physics, North-West University, Potchefstroom 2520, South Africa

<sup>2</sup> CNRS, Universite Paris 7, Denis Diderot, F-75205, 75005 Paris, France

**Summary.** In this review paper on pulsar wind nebulae (PWN) we discuss the properties of such nebulae within the context of containment against cross-field diffusion (versus normal advection), the effect of reverse shocks on the evolution of offset “Vela-like” PWN, constraints on maximum particle energetics, magnetic field strength estimates based on spectral and spatial properties, and the implication of such field estimates on the composition of the wind. A significant part of the discussion is based on the High Energy Stereoscopic System (*H.E.S.S.* or *HESS*) detection of the two evolved pulsar wind nebulae Vela X (cocoon) and HESS J1825-137. In the case of Vela X (cocoon) we also review evidence of a hadronic versus a leptonic interpretation, showing that a leptonic interpretation is favored for the *HESS* signal. The constraints discussed in this review paper sets a general framework for the interpretation of a number of offset, filled-center nebulae seen by *HESS*. These sources are found along the galactic plane with galactic latitudes  $|b| \sim 0$ , where significant amounts of molecular gas is found. In these regions, we find that the interstellar medium is inhomogeneous, which has an effect on the morphology of supernova shock expansion. One consequence of this effect is the formation of offset pulsar wind nebulae as observed.

## 1 Introduction

Even before the discovery of pulsars, pulsar wind nebulae (PWN) like the Crab Nebula were identified as belonging to a class of cosmic radio sources with relativistic electrons moving in magnetized plasmas to give the continuum radiation as observed. Visionaries like [37] already predicted that we should be able to measure the magnetic field strength in PWN using the combination of synchrotron and inverse Compton (IC) radiation. Following this, [44] were the first to provide us with a sophisticated one dimensional (1D) magneto hydrodynamical models (MHD) model of the Crab Nebula, which predicted a magnetic field strength distribution, consistent with broadband multiwavelength (radio through very high energy gamma-ray) constraints [23, 12, 40].

The discovery of the Crab pulsar in 1968 confirmed suspicions that a rapidly spinning neutron star should provide the energy input into the Crab Nebula, but soon questions concerning the spindown of pulsars in relation to the evolution of the nebulae arose. Whereas a few Crab-like remnants were discovered, Vela X, assumed to be associated with the 11,000 year old Vela pulsar, raised the question about the evolution of PWN as described by [64]. More serious evolutionary studies of PWN in supernova remnants (SNR) were launched by [55] and [56], but the offset of Vela X relative to the Vela pulsar raised the question if Vela X is indeed associated with the Vela pulsar. We also focus on Vela X in this discussion for the very specific reason that it serves as a prototype of evolved PWN. A wealth of new information on Vela X and similar evolved PWN became recently available as discussed in this review paper.

An excellent review of the structure and evolution of PWN from a radio and X-ray perspective was recently given by [34], whereas investigations on the population of galactic very high energy (VHE) H.E.S.S. sources considered to be associated with PWN were given by [47] and [35].

## 2 The evolving definition of pulsar wind nebulae (PWN)

The term “pulsar wind nebulae” (PWN), or “plerions” (derived from Ancient Greek *pleres*) – a term coined by [63], is described by the following:

- Filled center or blob-like form;
- A flat radio spectrum where the radio energy flux depends on frequency  $\nu$  as  $F_\nu \propto \nu^\alpha$ , with  $\alpha \sim 0$  to  $-0.3$ ;
- A well-organised internal magnetic field with high integrated linear polarisation at high radio frequencies.

The origins of the last property will be revisited in Section 6.

The main body of information on PWN came mainly from radio and X-ray observations, whereas interstellar absorption makes it difficult to detect most of these diffuse sources in optical as well. The study of PWN was therefore confined to a study of the synchrotron component only, which depends on the nebular field strength. This, and the fact that only radio and X-ray observations (representing widely divergent particle populations) have been used in theoretical studies, must have restricted progress in the understanding of PWN evolution and the conversion of spindown power into energetic particles in such nebulae.

With the growth of X-ray Astronomy, aided by sensitive instruments like *Chandra* and *XMM-Newton*, the definition of PWN has been broadened. We may add the following three important aspects

- A torus and jet near the pulsar, with the direction of the jet reflecting the direction of the pulsar spin axis and the torus showing an underluminous

region inside a characteristic scale radius  $R_s \sim 10^{17}\text{cm}$  to  $\sim 10^{18}\text{cm}$ , believed to be the pulsar wind shock radius (see [52] for parameter fits to such torii);

- Evidence for re-acceleration of particles somewhere between the pulsar light cylinder and  $R_s$ , leading to a hard X-ray spectrum with a photon index  $\sim 1.5$  to  $\sim 2$  near  $R_s$  (a review thereof will be given Section 4);
- Evidence for synchrotron cooling (spectral steepening) at  $R > R_s$ , with the size of the PWN decreasing towards increasing energies, as seen from the Crab and several other PWN. The photon indices of the cooled spectra range between 2.0 and 2.5 (see also Section 4).

The drawback of having only radio and X-ray synchrotron information on PWN was realised by [24, 31, 26], who were probably the first to predict that PWN evolved beyond the Crab phase (i.e. those would have field strengths smaller than the Crab) would accumulate sufficient amounts of relic electrons so that the inverse Compton (IC) scattering of these PWN electrons on the CMBR and possibly far infrared photons from galactic dust would be detectable by space and ground-based  $\gamma$ -ray telescopes. Furthermore, current generation ground based  $\gamma$ -ray telescopes have an angular resolution of a few arcminutes [41], so that the ratio  $\theta_{\text{PWN}}/\theta_\gamma$  of the PWN angular radius  $\theta_{\text{PWN}}$  relative to the telescope angular resolution  $\theta_\gamma$  increases to values greater than unity as the pulsar/PWN evolves beyond the Crab phase. They effectively become resolved, which allows us to measure spatially resolved spectra to the resolution of the VHE  $\gamma$ -ray telescopes. These complementary  $\gamma$ -ray observations then allow us to probe the electron spectra in the sources, as well as the associated magnetic field distribution, provided that comparable electron energies contribute to the observed (spatially resolved) synchrotron and IC spectra.

The H.E.S.S. telescope has the advantage of a large field-of-view, few arcminute angular resolution and good sensitivity against background rejection to probe extended sources [41] which allowed this telescope to see for the first time a population of evolved (resolved) VHE  $\gamma$ -ray emitting PWN [4, 8]. Such detections imply one or more of the following properties (see also [27]):

- The overall (total) wind magnetization parameter of the PWN  $\sigma_{\text{tot}}$  may be much less than unity (i.e. a particle dominated wind as discussed by [18], whereas [24] considered evolved PWN in equipartition. If the PWN is well below equipartition ( $\sigma_{\text{tot}} \ll 1$ ), synchrotron losses on the VHE emitting particles will be relatively small, leading to an intrinsically bright VHE source;
- Rapid expansion of the PWN during its early phases of high power input from the pulsar (such as G0.9+0.1 and the PWN of PSR B1509-58 [18]) results in a relatively low field strength in the PWN and hence the survival of the majority of VHE emitting electrons since early epochs. If the progenitor was part of an OB association, the combined stellar wind would blow a cavity so that the PWN expands nearly uninhibited for tens of kyr.

The magnetic field strength in such an expanded PWN can in principle drop below a few microgauss, so that synchrotron losses become less important relative to IC, ending up in a “dark VHE source”, since we can no longer rely on synchrotron emission to provide a multiwavelength counterpart. One such possibility is HESS J1303-631 which may be associated with Cen OB as reported by [5].

- The ideal condition (which includes the first two conditions) is to have the radiation lifetime  $\tau(E_\gamma)$  of VHE radiating particles comparable to, or longer than, the age  $T$  of the system, and therefore surviving even the earlier epochs when the field was stronger, so that the total amount of energy in electrons in the PWN is a significant fraction of the maximal rotational kinetic energy of the neutron star  $I\dot{\Omega}_0^2/2$  at birth. Only adiabatic losses are then the main source of losses. In this case we do not expect to see an energy dependence of the PWN size with changing  $\gamma$ -ray energy – a well known phenomenon for PWN where the lifetime of particles exceeds the age of the system. The predicted VHE  $\gamma$ -ray flux will then depend on the birth period of the pulsar.

The discovery of VHE  $\gamma$ -rays from HESS J1825-137 [6] and Vela X [7], both offset from their pulsars, confirm predictions of [61, 14, 33] that anisotropic reverse shocks can offset PWN from their original positions. We will discuss this further in this review paper. This conclusion led [27] to propose that a systematic investigation of middle-aged pulsars at the edges of resolved *center-filled* VHE  $\gamma$ -ray sources, combined with follow-up radio and X-ray imaging information, should result in the identification of a new class of PWN, with Ground-Based Gamma-Ray Astronomy taking the lead in this new direction. *GLAST* operations at its highest energies (where the angular resolution is best) is also expected to make a contribution to this field. In fact, with *GLAST* we expect to see a population of electrons with ages even longer than those seen by *HESS*.

[46] were the first to search for molecular clouds (based on CO and HI data) associated with such *HESS* sources, and in the case of HESS J1825-137, they found a cloud at the same kinematic distance to its associated pulsar PSR B1823-13. This cloud also has the correct orientation relative to the pulsar and  $\gamma$ -ray center of gravity to explain the observed offset in terms of an early reverse shock from the cloud location. A more detailed study on this topic was performed in the thesis of Lemière [47] whose study have revealed this new class of offset, filled center VHE PWN.

### 3 Energy scales and lifetimes of X-ray synchrotron and VHE IC emitting electrons

The IC scattering of VHE electrons on the 2.7K CMBR radiation is relatively efficient, since most scattering relevant to the observed VHE  $\gamma$ -ray range is

in the Thomson limit. Far infrared photons from galactic dust at an average temperature of 25K tend to preselect lower energy electrons where the Thomson limit still applies, whereas the cross-section for IC scattering decreases towards higher energies in the Klein-Nishina limit. The net effect is a steepening in the observed spectrum if far IR photons due to dust grains dominate, whereas the spectral index for IC in the Thomson limit is the same as that for synchrotron radiation by the same spectrum of electrons in a magnetic field. The reader is referred to the treatment by [15] on these topics.

In the prediction of a population of VHE  $\gamma$ -ray emitting PWN due to CMBR and far IR photons from dust, [24] remarked that the effect of dust would become more dominant towards the galactic center region. The most interesting application of this is the convincing prediction that a significant fraction of the galactic center H.E.S.S. source (HESS J1745-290) at the location of Sgr A\* is due to a pulsar wind nebula: The relativistic electrons of this PWN suffers severe energy losses as a result of inverse Compton scattering on the dense IR radiation field [42].

In the scaling equations below we will focus on the contribution from the CMBR alone, but refer the reader to [24, 28] for first order analytical Klein-Nishina corrections when including the dust component (also based on [15]).

The required electron energy in a transverse magnetic field of strength  $B = 10^{-5}B_{-5}$  G, to radiate synchrotron photons of mean energy  $E_{keV}$  (in units of keV) is given by

$$E_e = (70 \text{ TeV})B_{-5}^{-1/2}E_{keV}^{1/2}. \quad (1)$$

Similarly, the mean electron energy required to inverse Compton scatter the CMBR seed photons to energies  $E_{TeV}$  (in units of TeV) is typically lower at

$$E_e = (18 \text{ TeV})E_{TeV}^{1/2}. \quad (2)$$

The mean synchrotron photon energy (in units of keV) can be written in terms of the mean IC photon energy (following scattering on the CMBR)  $E_{TeV}$  (in units of TeV)

$$E_{keV} = 0.06B_{-5}E_{TeV}. \quad (3)$$

If we define the synchrotron lifetime ( $\tau = E/\dot{E}$ ) of a VHE electron in a transverse magnetic field  $B_{\perp}$ , scattering cosmic microwave background (CMBR) photons to energies  $E_{\gamma} = 10^{12}E_{TeV}$  eV (in the Thomson limit) can be shown to be

$$\tau(E_{\gamma}) \sim (4.8 \text{ kyr}) \left( \frac{B_{\perp}}{10^{-5} \text{ G}} \right)^{-2} E_{TeV}^{-1/2}. \quad (4)$$

Note that the constant above depends on the assumed pitch angle distribution of the electron relative to the magnetic field direction. For an isotropic distribution this constant becomes 7.6 kyr. Other constants will also be obtained if we define the final electron energy to be an arbitrary fraction of the

initial energy. Assuming Eqn (4), the corresponding lifetime of keV emitting electrons would be shorter:

$$\tau(E_X) = (1.2 \text{ kyr}) \left( \frac{B_\perp}{10^{-5} \text{ G}} \right)^{-3/2} E_{\text{keV}}^{-1/2}, \quad (5)$$

where  $E_{\text{keV}}$  is again the synchrotron photon energy in units of keV. Once again, the constant 1.2 kyr increases to 1.6 kyr if we assume isotropic pitch angles. In very extended nebular MHD flows it is possible to get field strengths below the typical  $3\mu\text{G}$  ISM value, in which case we should include inverse Compton energy losses on the 2.7K CMBR. Following [9] we also include a Klein-Nishina suppression factor (relative to the Thomson limit) of 2/3 for the H.E.S.S. range to give a lifetime for TeV emitting electrons of

$$\tau(E_\gamma) \sim \frac{(100 \text{ kyr})}{[1 + 0.144(B_{\mu\text{G}})^2]E_{\text{TeV}}^{1/2}}, \quad (6)$$

where  $B_{\mu\text{G}}$  is now the field strength in unit of microgauss. This hints at a terminating VHE lifetime of 100 kyr. Note however that the X-ray synchrotron surface brightness in such extended low-field environments may be well below detectable levels, in which case a PWN will only be visible in the  $\gamma$ -ray domain (via the IC process), whereas no radio, optical and/or X-ray (synchrotron) plerionic counterpart is found. **Furthermore, the parent neutron star’s thermal and/or non-thermal X-ray component(s) may also no longer be visible, since the lifetime of VHE emitting electrons may even exceed the neutron star’s cooling and non-thermal radiating timescales!**

Such  $\gamma$ -ray detections are expected to contribute to the growing population of *Unidentified Gamma-Ray Sources* or *Dark Accelerators/Sources*, but given our growing knowledge through experimentation and theory, we should eventually be able to lift these PWN to the status of “*gamma-ray pulsar wind nebulae* without multiwavelength counterpart.”

## 4 Particle acceleration at PWN shocks

Although electrons and positrons from magnetospheric electromagnetic cascades escape with relatively low energy from the pulsar light cylinder, where the ratio  $\sigma_L$  of electromagnetic energy density to particle energy density must be much larger than unity ( $\sigma_L \sim 10^4$  for the Crab pulsar [22] this  $\sigma$  parameter must reduce drastically beyond the light cylinder for two reasons: (i) [65] have shown that the Crab pulsar’s radio pulses would have been smeared unless the Lorentz factor of the  $e^\pm$  wind exceeds  $10^4$ ; (ii) Observations at the pulsar wind shock indicate that this ratio must have reduced to  $\sigma \sim 3 \times 10^{-3}$  for the Crab [44, 17], but in the range 0.01 to 0.1 for the Vela PWN shock [59, 17]. The reader is referred to [11] for a review of this particle energization process.

The first observational evidence of a pulsar wind nebular shock was seen in the Crab Nebula, where the observation of the underluminous region within  $\sim 10$  arcsec from the pulsar made it natural for [54] to associate the pulsar wind shock ( $R_s \sim 0.1$  pc) with the boundary of this region.

Even though energy is converted from fields to the bulk of the particle population between  $R_L$  and  $R_s$ , we require an additional mechanism to accelerate electrons and positrons to ultrarelativistic energies with an electron spectral index of  $\sim 2$  (see Section 5 for observational evidence). Recently [10] have shown that the fractional energy content in the accelerated  $e^- - e^+$  component increases with increasing energy content in upstream (unshocked) ultra relativistic ions. These authors also found that the ratio of accelerated  $e^+$  to  $e^-$  components become significantly more than unity as the upstream wind energy flux becomes ion dominated. The reader is also referred to [10] for a review of the literature on ion mediated lepton acceleration in pulsar wind shocks.

Another fundamental question regarding pulsar wind nebulae is the maximum energy to which  $e^- - e^+$  can be accelerated at a pulsar wind shock to produce the observed high energy synchrotron and inverse Compton radiation downstream of the shock? We will attempt to answer this question without restricting ourselves to the microphysics of the acceleration process.

This limit for low field strength pulsar wind shocks was first discussed by [39] who considered the gyroradius limit and by [25] for synchrotron limited acceleration as discussed below.

#### 4.1 The synchrotron limit

For any ion gyro resonant (as discussed before) or Fermi I type acceleration process in a relativistic pulsar wind shock, electrons and/or positrons can be accelerated at a rate as fast as the gyroperiod, as reviewed by [25]. The latter authors then balanced this rate with synchrotron losses for relatively strong fields to derive a maximum characteristic (cutoff) synchrotron energy (in the lab frame) of

$$E_\gamma(\text{max}) = \left(\frac{3}{4\pi}\right)^2 \left(\frac{hc}{r_0}\right) = (25 \text{ MeV}) \quad (7)$$

for electrons/positrons in such relativistic shocks. This limit reproduces the observed characteristic synchrotron cutoff energy of  $\sim 25$  MeV for the Crab Nebula as seen by *COMPTEL* and *EGRET* [25]. The corresponding 90% confidence interval for this cutoff is 15 MeV to 70 MeV.

We note that [1] approached this problem from a totally different perspective by calculating the electron cycle times upstream and downstream of a relativistic shock. They finally arrived at exactly the same expression (Eqn 7), or Eqn. (A2) of [25] within a factor of  $2\pi$ . [3] also extended this limit to account for synchrotron limited acceleration of protons and electrons by

considering an acceleration timescale given by a scale factor  $\eta$  times the gyroradius relative to  $c$ , so that Eqn (A2) of [25] is retrieved if we set  $\eta = 2\pi$  (gyroperiod timescale). His maximum for electrons is then

$$E_{\gamma}(\text{max}) = (160 \text{ MeV})\eta^{-1} \quad (8)$$

similar to [1]. EGRET observations of the Crab Nebula are however consistent with Eqn 7, or,  $\eta \sim 2\pi$  [25].

## 4.2 The gyroradius limit

For lower field strengths (i.e. PWN evolved beyond the Crab-like phase), where synchrotron losses no longer constrain the maximum electron energy, we generalise the gyroradius limit of [39], which states that the highest energy particles must still be contained in the shock at  $R_s$  while participating in the acceleration process. In other words, the gyroradius of particles with energy  $E_{\text{max}}$  should be significantly smaller than  $R_s$ , or,

$$r_L = \frac{E_{\text{max}}}{eB_s} = \epsilon R_s < R_s, \quad (9)$$

where  $\epsilon < 1$  is the required fractional size of  $R_s$  for containment during any Fermi or gyro resonant type of acceleration to provide the bright synchrotron radiation downstream of the pulsar wind shock. This result does not depend explicitly on the acceleration timescale, but relatively fast acceleration (relative to escape and radiation losses) will result in maximal values of  $\epsilon < 1$ , until containment becomes a problem.

We can again generalise this expression by adding the charge number  $Z$  ( $= 1$  for electrons and positrons) for the possible acceleration of ions to give

$$E_{\text{max}} = Ze\epsilon B_s R_s. \quad (10)$$

Eqn (10) converges to Equation (52) of [1] if we set the abovementioned containment factor  $\epsilon = (\ell_c/3r_L)^{1/2} < 1$ , where  $\ell_c$  is the coherence length of the field, if the latter is assumed to be randomly oriented. We, however, do not specify the exact physics of acceleration so that  $\epsilon$  is kept as a free parameter, which is constrained to be less than unity from a general containment principle.

We apply this constraint to PWN by using the [44] formalism to write the post-shocked field strength in terms of the pulsar spindown power and parameters related to the pulsar wind shock to give

$$B_s = \kappa \left[ \frac{\sigma \dot{E}}{(1 + \sigma)c} \right]^{\frac{1}{2}} \frac{1}{R_s}, \quad (11)$$

with  $\sigma$  the wind magnetization parameter ( $\sigma \equiv$  electromagnetic energy density to particle energy density at  $R_s$ ) and  $\dot{E}$  the spindown power of the pulsar. The



magnetic compression ratio  $1 < \kappa < 3$  [44] depends on the strength of this relativistic shock (and hence  $\sigma$ ). For strong shocks ( $\sigma \ll 1$ ) we have  $\kappa \sim 3$ , whereas  $\kappa \sim 1$  for weaker Vela-like shocks [44], where  $\sigma \sim 0.01$  to  $0.1$  [59, 17].

The expression for the maximum particle energy for remnants with field strengths weaker than the Crab (i.e. where radiation losses do not limit the energy) can now be written in terms of  $\sigma$  and  $\dot{E}$ , without having to know where the shock is located (since  $R_s$  cancels):

$$E_{\max} = \epsilon \kappa e \left( \frac{\sigma}{1 + \sigma} \frac{\dot{E}}{c} \right)^{1/2} = (110 \text{ TeV}) \kappa \left( \frac{\epsilon}{0.2} \right) \left( \frac{\sigma}{0.1} \dot{E}_{36} \right)^{1/2}, \quad (12)$$

where the spindown power has been rescaled in terms of a typical Vela-like value of  $\dot{E} = 10^{36} \dot{E}_{36}$  ergs/s and a Vela-like  $\sigma \sim 0.1$ . However, according to [39] the maximum energy is equal to the polar cap potential, in which case the term  $\epsilon \kappa \sigma / (1 + \sigma)$  should drop away (i.e. no field compression and magnetisation). In this case the maximum energy for a Vela-like pulsar would be  $\sim 350$  TeV if  $\epsilon = 0.2$ .

The discussion of this maximum is very relevant from an observational viewpoint, since the highest photon energy at any location in the PWN will always be bounded by such a quantity, which should evolve with time as a result of pulsar spindown.

### 4.3 PSR B1929+10: a challenge for particle acceleration in PWN shocks.

The aforementioned maximum electron energy imposes an important boundary condition when modelling the extended X-ray and  $\gamma$ -ray emission from PWN, since this maximum will suffer synchrotron and adiabatic losses during electron transport to the outer edge of the PWN. While this long-term transport process is taking place, the spindown power will also be decreasing with time, resulting in a decrease of  $E_{\max}$  at  $R_s$  for freshly injected electrons (making compact nebular X-rays) as well. For the sake of simplicity we will assume that the maximum electron energy is set by the pulsar polar cap potential [39].

The detection of an X-ray synchrotron trail from PSR B1929+10 by [62, 13] from X-ray observations should challenge the maximum electron energy set by Equation (12), since the spindown power  $\dot{E} = 3.9 \times 10^{33}$  ergs/s is low compared to even Vela-like pulsars. [13] considered the case where the time  $t = R_t / V_p$  (with  $R_t$  the length of the trail seen in X-rays and  $V_p$  the pulsar proper motion velocity) is equal to the synchrotron lifetime  $\tau_s$ , which can be several thousand years for a trail field strength  $B < 10 \mu\text{G}$ . Even if we assume that the electrons never lost any energy along their transport from  $R_s$  to the present weak-field trail location, we find from Equation (12) that the maximum electron energy is given by

$$E_{\max}(\text{B1929}) \sim (20 \text{ TeV}) \left( \frac{\epsilon}{0.2} \right), \quad (13)$$

whereas the corresponding characteristic synchrotron energy in a nebular magnetic field, normalised to a strength of  $B_{-5} = B/10\mu\text{G}$ , would be given by

$$h\nu_{\max}(1929) < (300 \text{ eV}) B_{-5} \left( \frac{\epsilon}{0.2} \right)^2. \quad (14)$$

This limit is clearly in the soft X-ray band, falling short to explain synchrotron emission up to 10 keV as observed.

If the pulsar has spun down significantly during a time  $t$  into the past, then we are looking at relic electrons in the trail, but accelerated at the pulsar wind shock when the age of the pulsar was equal to  $T - t$ , where  $T$  is the current true age. Assuming a pulsar braking index of  $n = 3$ , the *retarded spindown power* would then be

$$\dot{E} = \frac{\dot{E}_0}{(1 + (T - t)/\tau_0)^2}, \quad (15)$$

where  $\dot{E}_0$  is the spindown power at birth and  $\tau_0 = P_0/2\dot{P}_0$  the characteristic age at birth when the initial spin period was  $P_0$  and period derivative  $\dot{P}_0$ . For those not familiar with the concept of a *retarded spindown power*: The author borrowed this concept from electrodynamics where the term *retarded potential* is used to describe radiating systems, where the changing vector potential seen by the observer is the result of particle movement some time in the past. Also, for those not familiar with the concept of a *braking index*: The spindown power of a pulsar can be written as a function of the rotational frequency  $\Omega$  as  $-\dot{E} = K\Omega^{n+1}$ , where  $K$  depends on several neutron star properties and  $n$  the braking index. For magnetic dipole radiation and energy losses via particle outflow through the pulsar polar cap as in the well-known Goldreich-Julian model,  $n = 3$ . However, even this retarded spindown may not solve the problem of PSR B1929+10 since the age  $T = 3 \times 10^6$  years (i.e. already too large), so that quantity  $(T - t)/T \sim 1$  does not give us any advantage.

We can therefore only speculate about possible explanations for the existence of X-ray synchrotron photons from the trail of PSR B1929+10: One possibility is re-acceleration due to adiabatic compression in the bow shock. A detailed discussion of this is however beyond the scope of this general review paper, except to mention that more X-ray observations, as well as future ground based VHE  $\gamma$ -ray observations are important to characterise this important laboratory for particle acceleration. Whereas X-rays measure the convolution of the electrons with the field strength in the trail, the VHE  $\gamma$ -rays would directly probe the particle population via the IC scattering of this relic component on the CMBR and known far infrared photons from galactic dust grains.

## 5 The energy dependent cooling radius of a PWN

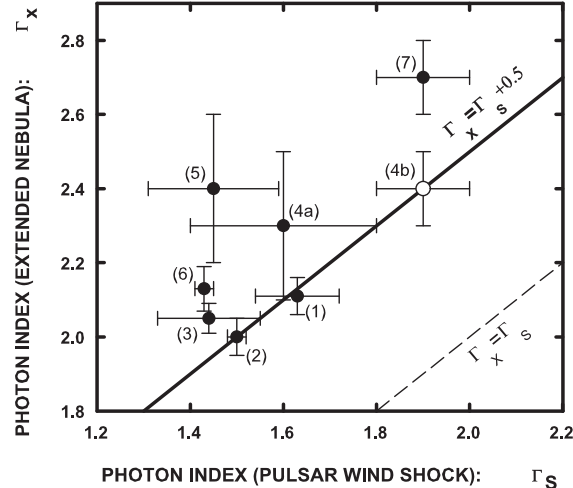


**Fig. 1.** Plot of the X-ray spectral index  $\Gamma_X$  around  $\sim 1$  keV at the maximal observable radius (or “extended nebula”) versus the spectral index  $\Gamma_s$  for the same energy range near the pulsar wind shock. The dashed line indicates  $\Gamma_X = \Gamma_s$  whereas the solid line represents the line  $\Gamma_X = \Gamma_s + 0.5$  expected for  $dE/dt \propto -E^2$  (e.g. synchrotron) cooling if we assume that the maximum observable photon energy is still above the upper spectral edge of the observations in the extended nebula (typically  $> 10$  keV). References: (1) Crab [36], (2) Vela [49, 50], (3) PSR B1509-58 [32], (4a) G18.0-0.9 [33], (4b) HESS J1825-137 [9], (5) G0.9+0.1 [53], (6) G21.5-0.9 [51], & (7) 3C58 [16, 58]

In Figure 1 we summarise the observed spectral steepening with radius  $r > R_s$ , where  $R_s = d\theta_s$  is the pulsar wind shock radius,  $d$  is the distance between earth and the pulsar, and  $\theta_s$  is the angular distance between the pulsar and its wind shock as seen on the sky: If  $\Gamma_s$  is the photon spectral index (as seen in X-rays) at the pulsar wind shock, a steepening  $\Gamma_x > \Gamma_s$  corresponding to  $r > R_s$  is observed as a result of radiative losses. This effect is mostly seen in the X-ray (synchrotron) domain, but may be less so in the VHE (IC) domain where lower energy electrons (producing the VHE  $\gamma$ -rays) suffer less radiative losses compared to the synchrotron emitting electrons.

Theoretically we would expect a convergent value of  $\Gamma_X = \Gamma_s + 0.5$  as a result of radiative (mostly synchrotron) cooling, since the energy loss rate scales as electron energy squared. It is clear that the points all lie either on this (solid) line in Figure 1, or above it. The reason for the latter is because the spectral cutoff associated with the highest energy electrons at the observed angular radius  $\theta_X$  may only contribute to energy bins below the upper

spectral edge used in the analysis, in which case the spectral index  $\Gamma_X$  may asymptotically diverge to relatively large numbers near  $\theta_X = r/d$ . However, even this information is useful in sophisticated models where the maximum electron energy in the PWN shock serves as one of the inputs. This can help us to constrain the maximum electron energy at  $\theta_s$  in time dependent models which takes the full evolution into account.

Any PWN has a terminating radius  $\theta_{\text{PWN}}$ , which pushes against the SNR ejecta, swept-up gas or ISM. This edge is usually seen in radio (if the PWN is also detectable in radio), because the lifetime of radio synchrotron emitting electrons is longest and they survive in the oldest expanding volume at the radial distance  $\theta_{\text{PWN}}$ . Suppose we define the angular radius  $\theta_{1/2}$ , with  $\theta_s < \theta_{1/2} \leq \theta_{\text{PWN}}$ , as that radius where  $\Gamma_X = \Gamma_s + 0.5$  is reached. We then define the energy dependent scaled cooling radius as

$$\xi_{1/2} \equiv \frac{\theta_{1/2}}{\theta_{\text{PWN}}}, \quad \text{where} \quad \frac{d\xi_{1/2}}{dE_e} < 0. \quad (16)$$

The scaled radius  $\xi_{1/2}$  should thus decrease towards increasing electron energies  $E_e$ . Although this is well-known, there is little experimental data to support this: Detectors with good angular resolution to resolve PWN also have limited bandwidth (typical 0.5 to 10 keV), but if the statistics are good enough, observers should consider splitting the data into two energy bands of equal statistics to identify a possible shift in  $\xi_{1/2}$  between the two energy bands.

In the Section 7 we will review the H.E.S.S. detection of the PWN G18.0-0.7 = HESS J1825-137 associated with the Vela-like pulsar PSR B1823-13, which clearly shows a similar steepening of the photon index with radius.

## 6 *Pleres pera* or “filled bags”

The most fundamental principle in PWN flows is that the pulsar wind slows down from relativistic to relatively low expansion velocities as a result of the confining pressure. This slow down typically occurs after the pulsar wind has been shocked at some distance  $R_s$  from the pulsar (see e.g. [44]). The decelerating post shock ( $r > R_s$ ) pulsar wind flow velocity  $\mathbf{V}$  would typically be radial, i.e.  $\mathbf{V} \sim V_r \mathbf{e}_r$ . Furthermore, the associated magnetic field at  $r > R_s$  would be described by the equation (see e.g. [44])

$$\nabla \times (\mathbf{V} \times \mathbf{B}) \sim 0, \quad (17)$$

in which case  $\mathbf{B} \sim B \mathbf{e}_\perp$ : The field direction would also be approximately perpendicular relative to the radial flow direction. The reader is probably familiar with the *Chandra* image of the Crab Nebula and other X-ray plerions, showing exactly the toroidal (azimuthal) structures implied by this vector Equation.

Given this introduction, we now raise two questions: (i) Is it possible for a high energy particle to overtake this convective flow as a result of diffusion? (ii) Under which conditions would it be possible for such a particle to escape through the boundary of a PWN? We will therefore compare radial diffusion versus radial convective flow, where the diffusion is *perpendicular* to the (e.g. toroidal) magnetic field line.

The most general form of the perpendicular diffusion coefficient is given by

$$\kappa_{\perp} = \frac{1}{3}\lambda_{\perp}c, \quad (18)$$

where  $\lambda_{\perp}$  is the mean free path for scattering in a direction which is perpendicular to the field line direction (i.e. cross field diffusion). The case we consider here therefore corresponds to diffusion in the radial direction relative to the pulsar. We parameterize this quantity further by writing it as a factor  $f$  times the particle gyroradius  $\rho_L$ , so that

$$\lambda_{\perp} = f(\Omega\tau)\rho_L, \quad (19)$$

where  $\Omega$  is the particle gyrofrequency and  $\tau$  is the mean time between scatterings. The *Bohm limit* corresponds to  $\Omega\tau \sim 1$  and  $f(\Omega\tau) = 1$ . Assuming hard sphere scattering, it can be easily shown for both weak scattering ( $\Omega\tau \ll 1$ ) and strong scattering ( $\Omega\tau \gg 1$ ) that  $f(\Omega\tau) \ll 1$  [60]. Thus, under the assumption of hard sphere scattering, the mean free path against diffusion perpendicular to a field line is always less or equal to the particle gyroradius. This is intuitively expected: It is difficult for charged particles to cross field lines - a principle we have learned from undergraduate days!

Scaling a PWN to a distance of  $d = 1d_{\text{kpc}}$  kpc with an age of  $\tau = 20$  kyr and an associated field strength of  $B = 3\mu\text{G}$ , we arrive at an angular spread due to diffusion of VHE electrons scattering CMBR photons in the Thomson limit to VHE  $\gamma$ -rays of energy  $E_{\text{TeV}}$  (from Eqn 2)

$$\theta_{\text{diff}}(e^{\pm}) = 0.07^{\circ} d_{\text{kpc}}^{-1} \left[ \left( \frac{f(\Omega\tau)}{0.1} \right) \left( \frac{3\mu\text{G}}{B} \right) \left( \frac{\tau}{10\text{kyr}} \right) \right]^{1/2} E_{\text{TeV}}^{1/4}. \quad (20)$$

Thus, the toroidal field line structures in PWN tend to contain relativistic particles much better than would have been the case if the field line structures had radial components, in which case the parallel diffusion coefficient is relatively large ( $\lambda_{\parallel} \gg \rho_L$ ). In the latter case much larger cosmic ray type diffusion coefficients would have been appropriate as employed by [2] for PSR B1706-44, so that relic charged particles accumulated over the source lifetime would have escaped much more easily from the convective plasma, with the latter reflected by the radio morphology.

We therefore conclude that PWN act as well-contained “filled bags” (or *pleres pera* in Ancient Greek) with high integrity against diffusion losses over Vela-like lifetimes. Such sources will expand convectively until the PWN pressure becomes small enough so that particles start to leak into the interstellar

medium. The same principle is also expected to hold for ultrarelativistic ions injected into the PWN over the lifetime of the PWN: If  $E_i$  is the total energy per ultra relativistic ion with charge  $X$ , the spatial ion spread due to diffusion alone is then

$$\theta_{\text{diff}}(\text{ion}) = 0.05^\circ d_{\text{kpc}}^{-1} \left[ \left( \frac{1}{Z} \right) \left( \frac{f(\Omega\tau)}{0.1} \right) \left( \frac{3\mu\text{G}}{B} \right) \left( \frac{\tau}{10\text{kyr}} \right) \left( \frac{E_i}{10\text{TeV}} \right) \right]^{1/2}. \quad (21)$$

If we claim that several of the unidentified filled-center H.E.S.S. sources near Vela-like pulsars in the galactic plane are PWN, diffusion would spread them by undetectable amounts (given the *H.E.S.S.* angular resolution of  $\sim 0.07^\circ$ ) relative to convective sizes  $\theta_{\text{PWN}}$ . For example, scaling the  $\sim 2$  degree convective size of the Vela X PWN to a distance of 1 kpc gives  $\theta_{\text{PWN}} = 0.3^\circ d_{\text{kpc}}^{-1}$ , which is large compared to the diffusive size.

## 7 HESS J1825-137 and the Three Princes of Serendip

The serendipitous discovery of the source HESS J1825-137 as part of the Galactic plane H.E.S.S. survey [4] serves as a good example of the correct use of the word *serendipity* as coined by Horace Walpole in the 18th Century, based on the old Persian tale of the *Three of Princes of Serendip*. In this story the rewards did not come at the time of discovery, but only later. We will also identify three main discoveries following the collection of sufficient statistics on this source.

The first H.E.S.S. observations of this region occurred as part of a systematic survey of the inner Galaxy from May to July 2004 (with 4.2 hours of exposure within  $2^\circ$  of HESS J1825-137). Evidence for a VHE  $\gamma$ -ray signal in these data triggered re-observations from August to September 2004 (5.1 hours), resulting in a significance of  $13\sigma$ . This led to the announcement by the H.E.S.S. Collaboration [6] of a possible association of this source with the Vela-like pulsar PSR B1823-13 and its associated PWN G18.0-0.7 as identified in X-rays by [33].

Further observations during 2005 resulted in improved statistics to study the energy dependent morphology [9]. One of the main reasons for this was to get full orbital coverage on the source LS 5039 as seen in Figure 2. The total lifetime then increased to 52.1 hours with a significance of  $34\sigma$ .

The three main discoveries with respect to HESS J1825-137 are the following:

### 7.1 The anomalously large size of HESS J1825-137 and its implied SNR shell

Since the X-rays already show the effect of full cooling from a photon index of  $\sim 1.6$  to  $\sim 2.3$  (Figure 1) within a distance of  $\sim 5$  arcmin from the pulsar [33],

we would expect that the X-ray PWN G18.0–0.7 already reached its terminal size. If this is not the terminal size, further cooling well beyond 5 arcmin should then result in  $\Gamma_X \gg 2.3$  as discussed in Section 4 accompanied by the loss of X-ray statistics.

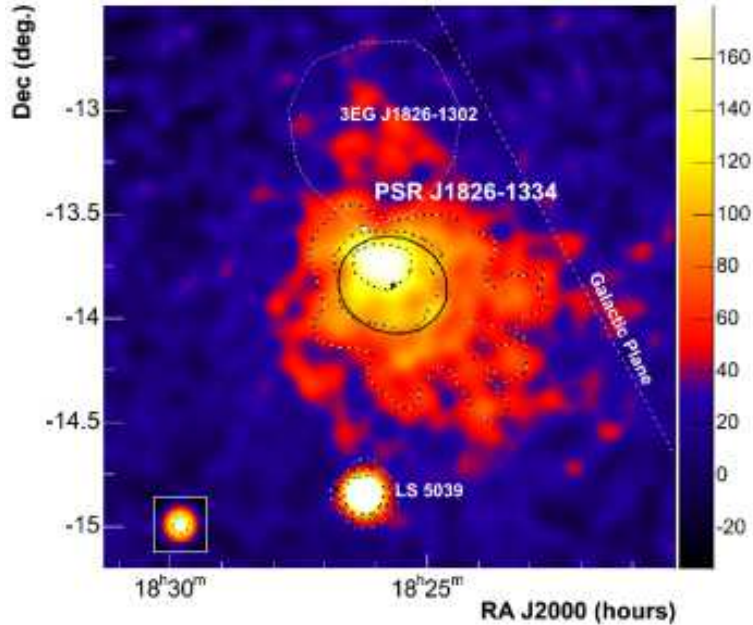


**Fig. 2.** Acceptance-corrected smoothed map of HESS J1825-137 [9] showing the extended emission relative to PSR B1823–13=PSR J1826–1334. The dotted line indicates the 95% confidence contour of the unidentified EGRET source 3EG J1826–1302. The point source at the bottom corresponds to the microquasar LS 5039. (Figure from [9].)

The VHE  $\gamma$ -ray size is however  $\sim 1^\circ$  as seen from Figure 1, which is much larger than G18.0–0.7 and the anomalously large size of the pulsar wind nebula can be explained if the pulsar PSR B1823–13 was born with a relatively large initial spindown power and braking index  $n \sim 2$ , provided that the SNR expanded into the hot ISM with relatively low density ( $\sim 0.003 \text{ cm}^{-3}$ ). This pulsar is a 101 ms evolved pulsar with a spin-down age of  $T = 2.1 \times 10^4$  years for an assumed braking index of  $n = 3$  [20] and in these properties very similar to the Vela pulsar. It is located at a distance of  $d = 3.9 \pm 0.4 \text{ kpc}$  [21].

The average VHE  $\gamma$ -ray radius of the PWN of  $\sim 0.5^\circ$  corresponds to  $R_\gamma = 35d_4 \text{ pc}$  for a distance of  $d = 4d_4 \text{ kpc}$ . Since the observed ratio of SNR forward shock radii to PWN radii are all a factor 4 or larger [61], the expected SNR forward shock radius  $R_{\text{SNR}} > 140d_4 \text{ pc}$ , making this one of the largest

expected SNR in our galaxy. de Jager et al. [29] derived a constraint on this forward shock radius, which can be stretched to a value of

$$R_{SNR} = (120 \text{ pc}) \left( \frac{E_{SN}}{3 \times 10^{51} \text{ ergs}} \frac{0.001 \text{ cm}^{-3}}{N} \right)^{0.2} \left( \frac{1}{n-1} \right)^{0.4}. \quad (22)$$

Finally, returning to the question about the apparent discrepancy between the VHE and X-ray sizes: We can achieve the observed ratio of 1 degree (VHE) relative to 5 arcmin (X-rays) easily in a low-B environment (with  $E_{\text{TeV}} \sim 0.3$  and  $E_{\text{keV}} = 1$ ) if we adopt the equation for conservation of magnetic flux in spherical coordinates (assuming the steady state solution, giving  $RVB = \text{const}$ ), and that the radius  $R$  is equal to the expansion velocity  $V$  times radiation lifetime. This would give a field strength in the outer VHE nebula, which is about 3 times smaller than the field strength in the smaller X-ray nebula. In fact, we do need a small field strength in the outer nebula to allow VHE emitting electrons to survive while producing a VHE spectral break as observed. The latter will also be covered in this review.

## 7.2 The offset PWN in X-rays and VHE $\gamma$ -rays

At the time of the X-ray discovery of G18.0-0.7, it was found that whereas the uncooled X-ray compact nebula is symmetric around the pulsar, the extended cooled nebula is offset to the south. To explain this offset, [33] introduced the reverse shock explanation of [14] for Vela X, where hydrodynamical simulations have shown that SNR expansion into an inhomogeneous medium would result in a reverse shock returning first from the region of higher density. After crushing the PWN, the latter is offset from its original position, resulting in a new center of gravity. We also observe that the entire VHE image is shifted relative to the pulsar (Figure 2) and the same explanation for HESS J1825-137 was also offered by us in [6].

By extending a line from this shifted VHE center of gravity through the pulsar, [47] discovered a molecular cloud in CO at a distance from earth, which is consistent with the dispersion based distance to the pulsar. This means that the SNR forward shock most likely struck this cloud, resulting in a reverse shock returning first to the expanding PWN of PSR B1823-13, which then resulted in a predictable offset direction for the VHE center of gravity.

Since this process takes of the order of 3 to 10 kyr to offset a PWN, we can expect several Vela-like PWN (with ages older than 10 kyr) to be offset in VHE  $\gamma$ -rays, since SNR expansion is always expected to take place in an inhomogeneous medium (i.e. the ISM is rarely expected to be homogeneous).



### 7.3 Energy dependent morphology and the cooling break

#### (a) Spectral steepening away from the pulsar

The most astonishing discovery of this source (given the extended statistics) was the discovery of a steepening spectrum as a function of increasing distance from the pulsar as described in [9] as shown on the left side of Figure 3, where we see the photon index in intervals of 0.1 degrees (along the sector of brightest emission) increasing from  $1.9 \pm 0.1$  to  $2.4 \pm 0.1$  at the outer part. The corresponding surface brightness for the same slice/sector is shown in the right-hand panel of Figure 3 and note the peak at a distance of  $0.15^\circ$  from the pulsar. We will revisit this feature below.

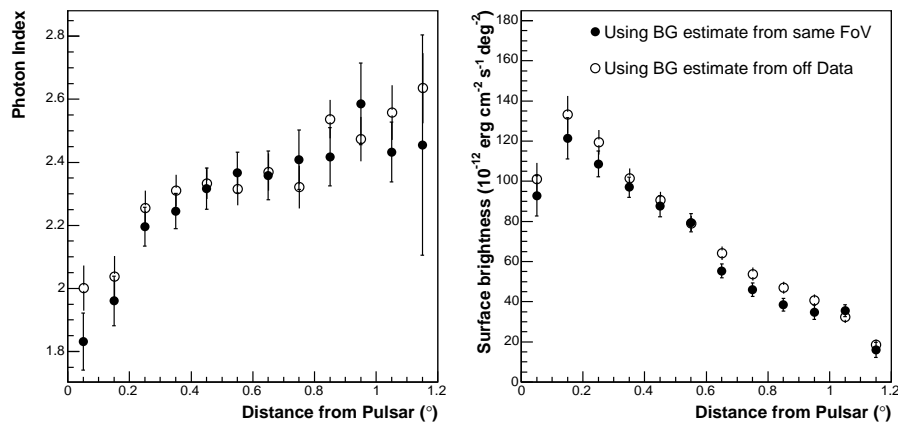


**Fig. 3.** **Left:** Photon index vs. radius along the sector of brightest emission from the pulsar as defined by [9]. **Right:** Relative surface brightness (all energies) corresponding to the left panel.

We can clearly see the energy dependence of the surface brightness with radius if we take the power law fits corresponding to each radial interval (from [9]) and calculate the relative surface brightness for energies chosen within the energy limits of the power law fits. The results are shown in Figure 4. Note that these relative surface brightness plots therefore represent smoothed averages over energy, whereas the radial scale remains uncorrelated.

In this plot we can see that the size of the source shrinks with increasing energy and that the peak surface brightness (corresponding to the shifted PWN due to the effect of the reverse shock) in Figure 3 is located at a radius of  $\theta_{\text{peak}} \sim 0.2^\circ$  from the pulsar for  $E_\gamma \sim 0.2$  TeV in Figure (4). This peak however shifts towards the pulsar for increasing energies (i.e.  $\theta_{\text{peak}} \leq 0.1^\circ$  for  $E_\gamma > 0.9$  TeV). Also, the relative surface brightness drops below the 50% level only for  $E > 0.9$  TeV.

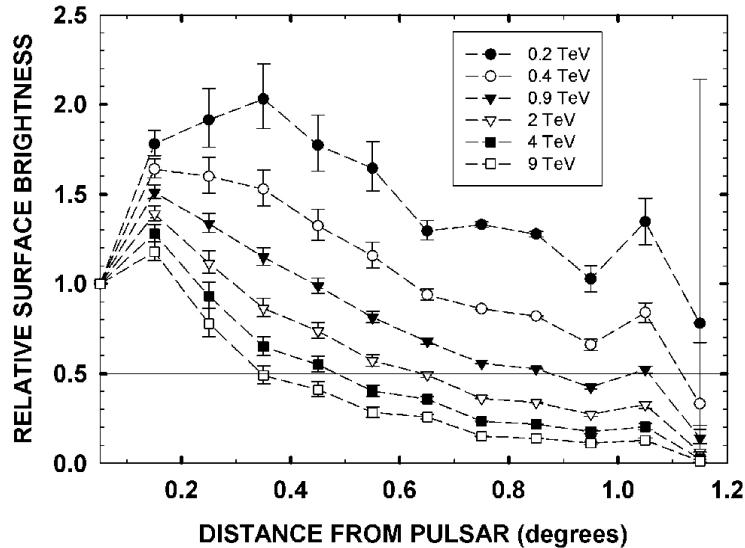


**Fig. 4.** Relative surface brightness versus distance from the pulsar for energies between 0.2 TeV and 9 TeV as indicated in the legend. The relative brightness along the energy scale is correlated (because these points and their errors were derived from power law fits to individual radial slices), whereas it is uncorrelated along the radial scale.

With this clear evidence of an energy-dependent morphology we also show the first color image in the history of Gamma-Ray Astronomy (Figure 5): Defining the three basic colors RGB as  $R \equiv [E_\gamma < 0.8\text{TeV}]$ ,  $G \equiv [0.8\text{TeV} < E_\gamma < 2.5\text{TeV}]$  and  $B \equiv [E_\gamma > 2.5\text{TeV}]$ , we could combine these colors in a single colour image showing the extended red image, which shrinks with increasing energy towards the blue nebula above 2.5 TeV close to the pulsar. Note that the point source LS 5039 shows up as a white image because of its broad band nature and the fact that it is a point source.

We are now also in a position to compare the scaled cooling radii  $\xi_{1/2}$  (Equation 16) between X-rays and VHE  $\gamma$ -rays: For X-rays  $\xi_{1/2} \sim 5'/1^\circ \sim 0.1$ , whereas  $\xi_{1/2} \sim 1$  as measured by H.E.S.S. Thus, clearly  $d\xi_{1/2}/dE_e < 0$  as required by Equation (16), where  $E_e$  is the electron energy, which is higher for X-rays than for VHE  $\gamma$ -rays, as required by Equations (2) and (1) for a relatively low magnetic field strength as motivated above. Furthermore, since  $\xi_{1/2}$  is already close to unity for the VHE (IC) domain, we expect that  $\xi_{1/2}$  should become undefined for the GLAST (IC) domain since the electron lifetime will become longer than the age of the system for all positions in the PWN – similar to the radio emission in the Crab Nebula below the spectral break of  $10^{13}$  Hz, which does not show any cooling effects anymore.

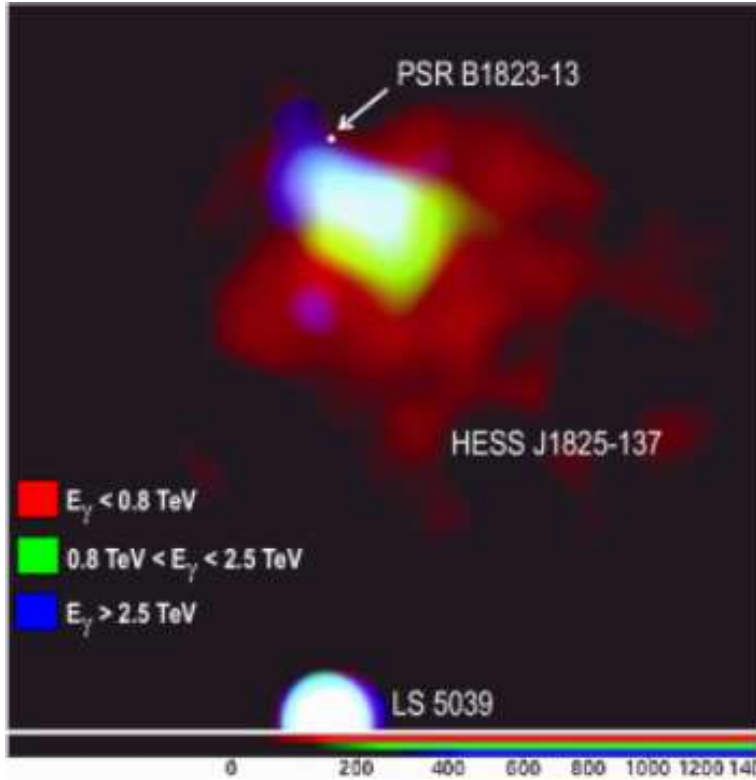


**Fig. 5.** First color image in the history of Gamma-Ray Astronomy showing the energy dependent morphology resolved in the three basic colors as indicated in the legend. The white point source at the bottom is the  $\mu$ -quasar LS 5039. Produced by S. Funk and O.C. de Jager for the H.E.S.S. Collaboration.

### (b) The cooling break in the total spectrum

The above mentioned behaviour is also summarised when we plot the total spectrum of HESS J1825-137 as shown in Figure 6, where we see that this photon spectral index steepens from  $\sim 1.9$  to  $\sim 2.6$  as expected for a cooling break. It is important to measure this cooling break, since we can then determine the average nebular field strength of the PWN, independently from a comparison of synchrotron and IC brightnesses, for which we do not have comparative data corresponding to the same electron energies. There are two problems if we attempt to “read” this break energy  $E_b$  from the energy spectrum as shown in Figure 6: (a) We do not know what the convergent (uncooled) photon spectral index below the H.E.S.S. range is, although this should be reflected by the synchrotron photon index ( $\sim 1.6$ ) of the uncooled electrons near the PWN shock. Therefore, most likely the electron spectral index for this domain is around 2.2. (b) Klein-Nishina effects due to dust IR photons tend to steepen

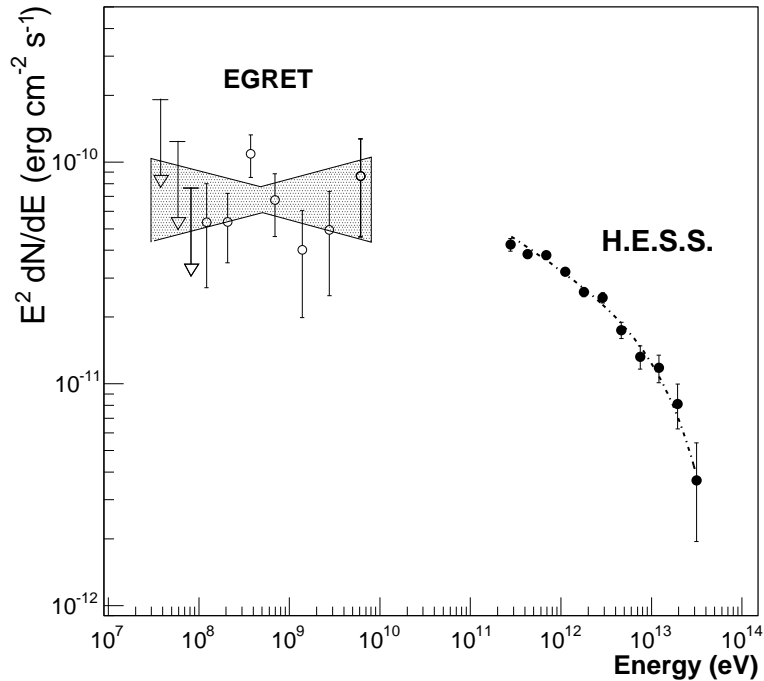


**Fig. 6.** The photon spectra of HESS J1825-137 and the nearby source 3EG J1826-1302 (multiplied by  $E^2$ ) showing the curvature in the spectrum of HESS J1825-137 [9].

spectra with increasing photon energy as described by [24] for such PWN. A more accurate procedure would then be either through direct modelling as done by [47] for HESS J1825-137, or, simply through fitting a two component electron spectrum scattering the CMBR and dust IR photons and rewriting the expressions for the cooling break directly in terms of the electron spectral break energy. Fortunately the estimate for the nebular field strength depends weakly on  $E_b$  as discussed below:

The anomalously large size of the unseen SNR forward shock radius is best met if the pulsar braking index  $n$  is closer to 2 than 3, giving a pulsar spindown age

$$T_p = (40 \text{ kyr}) \left( \frac{1}{n-1} \right), \quad (23)$$

which is closer to 40 kyr, rather than the canonical 20 kyr. It is possible to probe the field strength in most of the PWN volume by solving the expression

$$- \int_{E(\text{max})}^E \frac{dE_e}{(dE_e/dt)_s + (dE_e/dt)_{IC}} = T_p \quad (24)$$

for the electron energy  $E_e$ , where we include both synchrotron and inverse Compton losses [15]. In this case electrons injected with the maximum energy  $E_e(\text{max})$  at the PWN shock during the earliest epochs (when the spindown power was a maximum, see Section 4), move with the outer edge of the PWN. While losing most energy in the PWN, they must still be able to radiate VHE photons with energy at least  $\sim 4$  TeV to account for the highest energy spectral point at a distance of  $\sim 1$  degree from the pulsar as shown in Figure 4 of [9].

For inverse Compton energy losses on the 2.7K CMBR we include a Klein-Nishina suppression factor (relative to the Thomson limit) of  $2/3$  in the H.E.S.S. range [9]. By setting the spindown age equal to the total radiation lifetime of VHE  $\gamma$ -ray emitting electrons, we can write the electron energy in terms of the VHE  $\gamma$ -ray energy (Eqn 2) to give the observed spectral break energy of  $E_b \sim 2.5$  TeV [47], which is observed as a steepening in Figure (6):

$$E_b = \frac{(6.2 \text{ TeV})(n-1)^2}{[1 + 0.144(B_{\mu\text{G}})^2]^2}. \quad (25)$$

Thus, for  $n = 2$  ( $T = 40$  kyr age) and a  $B \sim 2\mu\text{G}$  field, the VHE  $\gamma$ -ray break would be around 2.5 TeV, whereas for  $n = 3$  (i.e. a  $T = 20$  kyr age), the required field strength would be  $3.9\mu\text{G}$ . Whereas [47] found the abovementioned break energy from broad band modelling of HESS J1825-137, GLAST should be able to measure the uncooled spectral index at  $\gamma$ -ray energies  $E_\gamma \ll E_b$ , which will allow us to constrain  $E_b$  more accurately in future.

#### 7.4 Conclusion: A particle dominated wind in HESS J1825-137

With both the spectral break around a TeV and the survival of  $\sim 5$  TeV emitting electrons to the edge of the PWN, it is clear that we require a magnetic field strength  $B < 3\mu\text{G}$  in the extended nebula. Such a low field strength also supports the relatively low observed X-ray to VHE  $\gamma$ -ray luminosity. A detailed treatment of this is however beyond the scope of this paper.

A concern which may be raised from a lay perspective: We know that the field strength in the ISM is about  $3\mu\text{G}$  or more, then why do we get an apparent field strength below this value?

The total pressure in the PWN is the sum of the magnetic pressure plus particle pressure, and we can already derive the total particle pressure from the electron spectrum responsible for the *HESS* signal: [30] derived the pulsar pair production multiplicities from the *HESS* data alone, as well as an upper limit by extrapolating the *HESS* spectrum along the harder uncooled pre-break  $e^+ - e^-$  spectrum with an index of  $\sim 2$  down to  $E_0 \sim 1$  GeV [30]. The total energy in electrons in the H.E.S.S. range is  $\sim 10^{48}$  ergs, but if we take the total energy down to  $E_0$  also into account, the total energy would be  $E_\pm \sim 8 \times 10^{48}$  ergs. This would have required a pulsar birth period  $2\pi/\Omega_0 = P_0 < 50$  ms to give a total rotational kinetic energy of  $0.5I\Omega_0^2 > E_\pm$ .

The total energy density in leptons is then  $U_e \sim (1 \text{ eV/cm}^3)d_4^{-3}$  for a PWN radius of  $0.5^\circ$ . The accuracy of this number is expected to improve when GLAST observations are added, which should measure the spectral hardening well below the break with better accuracy. The energy density in a  $B = 2 \mu\text{G}$  PWN field is  $U_B = (0.1 \text{ eV/cm}^3)(B/2 \mu\text{G})^2$ . Thus, to a first order we find that  $U_e \sim 10U_B$ , so that

- The PWN of HESS J1825-137 is particle dominated with lepton energy density about 10 times the field energy density, thus adding this PWN to the [18] list of particle dominated winds;
- The pressure  $U_e$  still appears to be significant to press against the ISM medium, which resulted in the anomalously large PWN as observed today.

## 8 Vela X – The prototype for evolutionary studies

Vela X, the bright flat spectrum radio component of the Vela SNR served as the prototype PWN for evolutionary studies [64]. The offset of the radio nebula to the south of the pulsar had Astronomers doubting if this association is real, until ROSAT discovered a cocoon of X-ray emission, also extending south of the pulsar, and aligned with a bright radio filament in Vela X [48]. The length of both features to the south is  $\sim 45'$ . More revealing was that even though this is one of the brightest polarised radio filaments, the degree of polarisation is low ( $\sim 15\%$  to  $20\%$ ). The reason for this is the presence of thermal material mixed into the plasma of highly relativistic particles [48]. A natural explanation for this two-fluid mixing and offset to the south was offered by [14] for Vela X: The reverse shock returning from a denser ISM offsets the PWN to the south while forcing this two-fluid mixing. Further evidence for this mixing came from the combined ASCA/ROSAT analysis of the bright cocoon (radio filament) region by [50] which shows evidence of mixing of a non-thermal component with photon index of  $\sim 2$  with a thermal component. Analyses by [43] with new ASCA results, as well as *XMM-Newton* observations of the cocoon of Vela X also confirmed this two-component spectrum [45].

### 8.1 H.E.S.S. detection of the Vela X “cocoon” – radio & X-ray correlation

The High Energy Stereoscopic System of telescopes observed the Vela region and discovered a structure resembling the Vela X cocoon in X-rays [7] as shown in Figure (7). The relative sizes however differ significantly: Whereas the size of the X-ray cocoon is  $45 \times 12 \text{ arcmin}^2$ , the corresponding VHE cocoon size is  $58 \times 43 \text{ arcmin}^2$ .

To complete the multiwavelength comparison, we also compare the VHE detection with the radio map: Figure (8) shows an overlay of the *HESS*  $\gamma$ -ray contours on the 8.4 GHz radio map of Vela X [48, 38], showing that

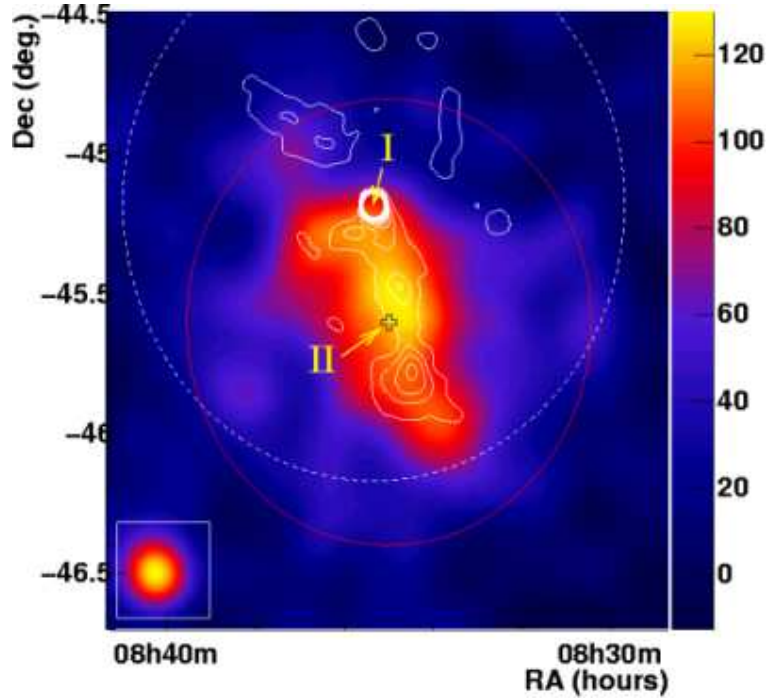


**Fig. 7.** Gaussian smoothed sky map of region surrounding Vela pulsar, showing significant emission to the south of the pulsar position, coincident with an X-ray feature seen by ROSAT PSPC (white contours). The solid circle represents the H.E.S.S. integration region for the spectral measurement, while the dashed circle represents the field of view for the ROSAT observations. (From [7]; see also this paper for more details).

the  $\gamma$ -ray map does overlap with the bright radio filament, which in turn overlaps with the X-ray cocoon as remarked by [48]. The latter author made the following observation based on the [57] model: The radio filaments are the result of Rayleigh Taylor instabilities in the SNR expansion. We conclude further that these filaments were also offset to the south of the pulsar by the early reverse shock. If the  $\gamma$ -ray signal is then due to hadronic interactions with this thermal gas, we would also expect to see a correlation between the  $\gamma$ -ray and filamentary structures.

The approximate full size of the Vela X PWN is  $\sim 3^\circ$  in RA and  $\sim 2^\circ$  in DEC as seen from a  $8^\circ \times 8^\circ$  HartRAO radio map of the Vela region at 2.3 GHz by Jonas (2006, personal communication). Note that the status of VHE  $\gamma$ -radiation from Vela X as a whole was not discussed by [7], although this total flux cannot be much larger than that from the VHE cocoon itself. We can then summarize the morphological multiwavelength properties of the cocoon detection as follows:

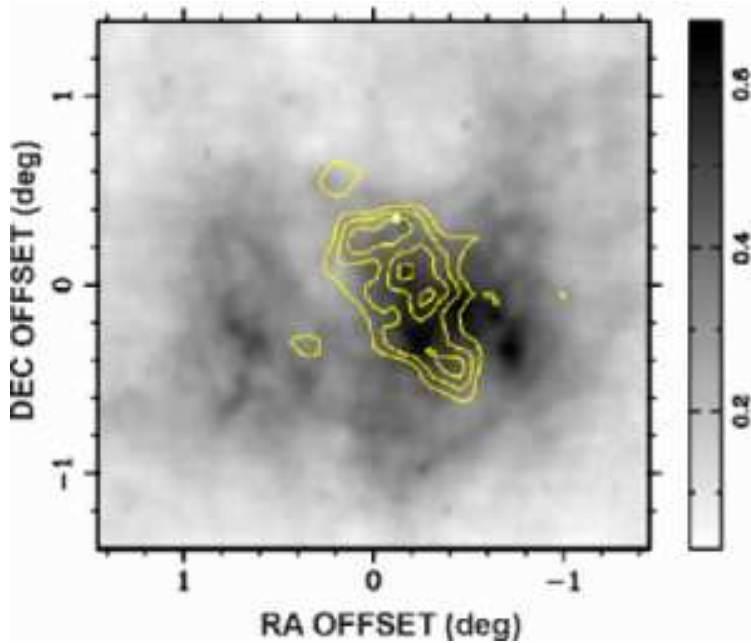


**Fig. 8.** Destriped radio image of Vela X at 8.4 GHz in greyscale [38] with the *HESS* map in Figure (7) converted to contours, overlaid in yellow. The pulsar position is marked by a white circle. The origin (zero point) of this image is (RA,DEC) = (129.02°, -45.54°) (J2000), which is different from the origin defined by [38].

- The volume of the VHE  $\gamma$ -ray cocoon is  $\sim 5\%$  relative to the total volume of Vela X;
- The cocoon contains both a non-thermal and thermal component, which is indicative of a reverse shock mixing gases of adiabatic indices  $\gamma = 4/3$  and  $5/3$  during the crushing phase;
- The offset of the cocoon to the south of the pulsar is explained by the reverse shock crushing the PWN to the south (see next Section);
- The position angle (P.A.) of the VHE  $\gamma$ -ray cocoon ( $41 \pm 7$  degrees, measured from north through east) is similar to that of the X-ray cocoon orientation (see next Section).
- The X-ray cocoon overlaps in position with a bright radio filament, although there are other similarly bright radio filaments further to the west without any X-ray or VHE  $\gamma$ -ray counterparts;
- Deeper, but wide FoV VHE observations of the entire Vela X structure shown in Figure (8) should indicate if there are  $\gamma$ -rays with lower surface brightness compared to the bright cocoon region.



## 8.2 Constraints on the cocoon field strength from the upper synchrotron cutoff energy

Since the cocoon has been shifted to the SW of the pulsar by the reverse shock, the highest energy electrons mixed in the thermal gas in the cocoon provide a powerful diagnostic of the age since shift and associated field strength. [50] measured a power law component up to at least 7 keV from the cocoon area. [43] and [45] also confirmed this two-component composition with *ASCA* and *XMM-Newton* observations respectively.

This means that ultrarelativistic electrons and thermal gas were mixed during the reverse shock crushing phase and with the offset PWN, the relativistic component is removed from its pulsar source, so that the upper spectral cutoff energy moves down in energy with time, without any source of replenishment. From Fig. 3 of [43], it is clear that this cutoff is currently  $\sim 10$  keV. The electrons radiating at this cutoff are not replenished by the Vela pulsar, since they have already been removed from the pulsar over a time interval  $T - T_c$ , which represents the time between the southward shift of the PWN from the pulsar (at time  $T_c$ ) and the present time  $T$ . These 10 keV emitting electrons were also the highest energy electrons accelerated by the PWN shock at the epoch  $T_c$  when the reverse shock started to crush the PWN. For such high energy electrons, IC scattering would be in the extreme Klein-Nishina limit, so that we only consider synchrotron losses, giving the time interval between the time of crushing and the present time of

$$T - T_c = (2.3 \text{ kyr}) \left( \frac{3 \mu\text{G}}{B} \right)^{3/2} \left( \frac{10 \text{ keV}}{E_{X(\text{max})}} \right)^{1/2}. \quad (26)$$

For Vela X [14] calculated  $T_c \sim 3$  kyr, whereas 2-D time dependent MHD simulations for the Vela SNR shows that the reverse shock was expected to reach the pulsar position around 5 kyr after the birth of the pulsar. Thus, a field strength around  $3 \mu\text{G}$  (or smaller) in the cocoon of Vela X is required to allow 10 keV synchrotron emitting electrons to survive between the time of crossing of the reverse shock and the present epoch. If the field strength was  $10 \mu\text{G}$  or larger (as required by [43] these electrons had to be shifted within 400 yr, which is unlikely to be achieved given any realistic reverse shock parameters.

## 8.3 Diffusion of VHE particles from the cocoon

[43] considered the problem of diffusion of X-ray synchrotron emitting electrons away from the X-ray cocoon, stating that a high field strength is required to contain the ultrarelativistic electrons in the  $45 \times 12$  arcmin<sup>2</sup> cocoon. Assuming that the cocoon is still expanding under its own pressure, a perpendicular field component is expected to be maintained by virtue of Eqn (17), so that Eqn (19) with  $f \ll 1$  for  $\Omega\tau \ll 1$  or  $\Omega\tau \gg 1$  is expected to hold, which protects the integrity of this PWN against diffusive escape. Replacing the time

$T - T_c$  with Eqn (26) in the diffusion equation, the electron energy cancels, so that the angular spread due to diffusion at a distance of  $d = 0.3$  kpc can be written as

$$\theta_{\text{diff}} = 0.5^\circ \left( \frac{f}{0.1} \right)^{1/2} \left( \frac{3 \mu\text{G}}{B} \right)^{3/2} \quad (27)$$

With a minimum X-ray cocoon dimension of 0.2 degrees, it is clear that we have to set  $f < 0.02$  for  $B = 3.3 \mu\text{G}$ , which places a restriction on the scattering parameter  $\Omega\tau$  based on hard-sphere scattering [60].

#### 8.4 No “missing” leptonic component in Vela X

[43] suggested that there is a missing leptonic component in Vela X. Whereas this is true for the cocoon, the actual volume of the Vela PWN (called “Vela X”) is about 20 times larger than the size of the cocoon as seen in VHE and to get the total energy in leptons, we have to take the bolometric spectrum from the total Vela X, which is one of the brightest radio nebulae in the sky. Using the radio spectrum of Vela X, [30] found that the total lepton energy in the radio nebula is  $W_e = 6.2 \times 10^{47}$  ergs (for  $B = 10 \mu\text{G}$ ) or  $3.8 \times 10^{48}$  ergs ( $B = 3 \mu\text{G}$ ), giving respective conversion efficiencies of  $W_e / (0.5 I \Omega_0^2) = 5\%$  and 30% for a birth period of 40 ms [61]. Thus, there does not appear to be a “missing” leptonic component and it is clear is that most lepton energy has been processed in the low energy leptonic domain. However, there are also observational lower limits to the Vela X averaged field strength: Using EGRET upper limits, [26] have shown that we can already constrain the volume averaged field strength to  $\langle B \rangle > (4 \mu\text{G})(\nu_b / 10^{11} \text{ Hz})^{0.4}$  where  $\nu_b$  is the unknown radio spectral break frequency. GLAST/LAT observations should either detect this radio counterpart of Vela X, or, provide more stringent lower limits on  $\langle B \rangle$ . This also calls for a separate study on variations in  $B$ : How does  $B$  in the cocoon differ relative to  $\langle B \rangle$ , given the presence of filaments in the PWN as well as the filling factor question?

#### 8.5 The H.E.S.S. signal: hadrons or leptons?

In the previous two sections we have shown the field strength in the cocoon must be relatively low for X-ray emitting electrons to survive at the southern tip of the cocoon, which would argue for an IC origin. This also implies a limit on the scattering parameter  $\Omega\tau$  for containment against diffusion through a weak perpendicular field. We have no theory to predict this number, but future research on turbulence theory may be able to make some predictions.

Another potential problem with a hadronic interpretation is the following: With the high required ion energy budget of  $10^{48}$  ergs (iron) to  $10^{49}$  ergs (protons) in the VHE cocoon, [43] invoked the early epoch of pulsar output to account for the observed  $\gamma$ -ray flux via hadronic interactions. However, protons ejected during such early epochs (and convected by the pulsar wind)

should fill the total (old) radio emitting Vela X PWN and not just the smaller (and younger) cocoon. Thus, the total energy budget in Vela X implied by the *H.E.S.S.* detection will then be (to a first order) 20 times larger than calculated for the cocoon:  $\sim 2 \times 10^{49}$  ergs (for iron) to  $2 \times 10^{50}$  ergs (for protons). Furthermore, [61] estimated a birth period of  $P_0 \sim 40$  ms for the Vela pulsar to account for the observed classical ratio of PWN radius to SNR radius of 0.25. The total integrated kinetic energy provided by the pulsar since birth is then  $0.5I\Omega_0^2 = 1.2 \times 10^{49}$  ergs, which means that we may have a conversion efficiency of  $> 100\%$  of spindown power to ions in Vela X. Thus, the VHE signal is more likely to be of leptonic than hadronic origin.

### 8.6 The VHE $\gamma$ -ray spectral break in the Vela X cocoon

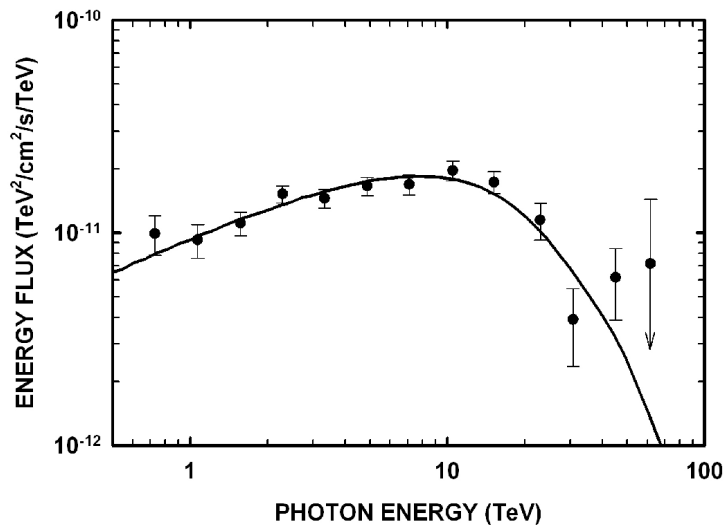


**Fig. 9.** Energy spectrum of the Vela X cocoon as measured by H.E.S.S. [7], with integration area shown in Figure 7. The solid line represents a fit assuming an inverse Compton origin as specified in the text.

If we assume that the H.E.S.S. signal is due to IC scattering on the CMBR in a relatively weak field of  $B \sim 3\mu\text{G}$ , then we should be able to predict the cooling break as that energy where radiation losses become comparable to the age of the PWN/SNR. This may then explain the spectral break in Fig. (9): In this case Eqn (25) would predict a VHE  $\gamma$ -ray spectral break energy of  $E_b \sim 12$  TeV for such a field strength, given a total age of 11 kyr. Note that this break energy  $E_b$  evolves downward in energy with time, and if we assume that the cocoon field strength did not change significantly over the past few

thousand years, the break energy is predicted to be

$$E_b = \frac{(15 \text{ TeV})}{[1 + 0.144(B/3 \mu\text{G})^2]^2} \left( \frac{11 \text{ kyr}}{T} \right)^2. \quad (28)$$

Note also that Fig. 9 represents *the first detection of a spectral maximum in VHE  $\gamma$ -ray Astronomy*, which allows this clear measurement of a spectral break energy.

## 9 Summary

In this review paper of pulsar wind nebulae (as seen by H.E.S.S.), we attempted to interpret the observed properties within a unified framework: We first reviewed the known properties of PWN as derived over many years from radio, IR, optical and X-ray observations. We then introduced new properties which are expected to make PWN bright high-energy to VHE  $\gamma$ -ray sources: For example, if the energy density in the soft radiation field (acting as target for IC scattering) dominates the energy density of the magnetic field, electron energy losses would be dictated by the IC rather than the synchrotron process. This principle is demonstrated when we compare the general properties of H.E.S.S. PWN with the Crab Nebula: The Crab Nebula is an efficient synchrotron radiator but inefficient  $\gamma$ -ray emitter (i.e. a high ratio of optical/X-ray energy flux to VHE  $\gamma$ -ray flux) as a result of the relatively large magnetic field energy density, but for most other H.E.S.S. PWN, the ratio of synchrotron to IC energy fluxes are comparable to, or even less than unity. This then hints at a relatively small magnetic energy density. Furthermore, in such cases we may also find that the energy density in relativistic electrons dominates the magnetic energy density, leading to the description of “**particle dominated winds**”, as opposed to the Crab Nebula which is known to be in equipartition.

We then reviewed the  $\gamma$ -ray lifetimes of PWN by considering electrons losing energy due to both synchrotron and inverse Compton radiation in the expanding post-shocked flow. As the PWN expands well beyond its X-ray phase (this X-ray phase terminates when the overall field strength becomes too small as a result of expansion), IC losses on the CMBR is then expected to dominate, in which case the terminating lifetime would converge to a value of 100 kyr. **Thus, if we observe a PWN at an energy near 1 TeV, the lifetime of the PWN is expected to be  $\leq 100$  kyr.** This discussion naturally led to the concept of particle spectral steepening as a function of increasing radius, but only as long as either synchrotron or IC radiation dominates the electron energy loss process.

The concept of dispersion in a PWN was also discussed: Is the observed size of a PWN mostly due to post-shocked convective (pulsar wind) flow, or, would diffusion dominate the process? At first glance (from this review paper)

it seems as if the ordered magnetic field in a PWN would inhibit dispersion due to diffusion. The result of this is that the expanding PWN "bubble" contains its radiating charged particles, but only as long as the magnetic field direction maintains its perpendicular direction relative to the radial direction. This question is relevant if we want to calculate the luminosity of a PWN as a function of time.

This review paper then concluded with a discussion of two important H.E.S.S. sources, where aspects such as (i) size, (ii) spectral energy distribution (SED) maximum, (iii) the offset of the center of gravity (of the VHE emission) relative to the pulsar position as a result of SNR expansion into an inhomogeneous interstellar medium, (iv) energy dependent morphology (i.e. the effect of spectral steepening in the radial direction) and (v) the observed VHE spectral break were discussed (if interpreted as the SED maximum). For both these sources it appears as if IC losses dominate over synchrotron losses, which has the advantage that the age of the PWN can be relatively accurately determined from the observed VHE spectral break: Assuming this, we showed that we indeed get consistent ages for both *H.E.S.S.* sources.

## 10 Acknowledgements

The first author acknowledges support from the South African Department of Science & Technology and National Research Foundation Research Chair: Astrophysics & Space Science. Support from the GDRI-GREAT French, German, South African & Namibian multinational funding source is also acknowledged. The authors would like to thank members of the Supernova Remnant, Pulsar and Plerion working group of the H.E.S.S. collaboration for useful discussions.

## References

1. Achterberg, A., Gallant, Y.A., Kirk, J.G., et al. , 2001, *MNRAS*, 328, 393
2. Aharonian, F.A., Atoyan, A.M. & Kifune, T. 1997, *MNRAS*, 291, 162
3. Aharonian, F.A. 2000, *New Astronomy*, 5, 377
4. Aharonian, F.A., et al. (H.E.S.S. Collaboration), 2005a, *Science*, 307, 1938
5. Aharonian, F.A., et al. (H.E.S.S. Collaboration), 2005b, *A&A*, 439, 1013
6. Aharonian, F.A., et al. (H.E.S.S. Collaboration), 2005c, *A&A*, 442, L25
7. Aharonian, F.A., et al. (H.E.S.S. Collaboration), 2006a, *A&A*, 448, L43
8. Aharonian, F.A., et al. (H.E.S.S. Collaboration), 2006b, *ApJ*, 636, 777
9. Aharonian, F.A., et al. (H.E.S.S. Collaboration), 2006c, *A&A*, 460, 365
10. Amato, A. & Arons, J. 2006, *ApJ*, 653, 325
11. Arons, J. 2004, Acceleration and Dissipation in Relativistic Winds, In *Young Neutron Stars and Their Environments*, IAU Symposium no. 218, Sydney, Australia. Ed. by Fernando Camilo and Bryan M. Gaensler. San Francisco, CA: Astronomical Society of the Pacific, p.163

12. Atoyan, A.M. & Aharonian, F.A. 1996, MNRAS, 278, 525
13. Becker, W.E., Kramer, M., Jessner, A., et al. , 2006, ApJ, 645, 1421
14. Blondin, J.M., Chevalier, R.A. & Frierson D.M. 2001, ApJ, 563, 806
15. Blumenthal, G.R. & Gould, R.J. 1970, Rev. Mod. Phys., 42, 237
16. Bocchino, F., Warwick, R.S., Marty, P., et al. , 2001, A&A, 369, 1078
17. Bogovalov, S.V., Chechetkin, V.M., Koldoba, A.V., et al. , 2005, MNRAS, 358, 705
18. Chevalier, R.A. 2004, Adv. Space Res., 33, 456
19. Chu, Y.-H., Kim, S., Points, S.D., et al. , 2000, AJ, 119, 2242
20. Clifton, T.R., Lyne, A.G., Jones, A.W., et al. , 1992, MNRAS, 254, 177
21. Cordes, J.M. & Lazio, T.J.W. 2002, unpublished (Astro-ph/0207156)
22. Coroniti, F.V. 1990, ApJ, 349, 538
23. de Jager, O.C. & Harding, A.K. 1992, ApJ, 396, 161
24. de Jager, O.C., Harding, A.K., Baring, M., et al. , 1995, Gamma-Ray Plerions, in Proc. of the 24th Int. Cosmic Ray Conf., OG 2, 528
25. de Jager, O.C., Harding, A.K., Michelson, P.F., et al. , 1996a, ApJ, 457, 253
26. de Jager, O.C., Harding, A.K., Sreekumar, P., et al. , 1996b, A&AS, 120, 441
27. de Jager, O.C. & Venter, C. 2005a, in "Towards a Network of Atmospheric Cherenkov Detectors VII, Cherenkov 2005 Proceedings", ed. B. Degrange, G. Fontaine. (astro-ph/0511098)
28. de Jager, O.C. 2005b, H.E.S.S. Observations of Pulsar Wind Nebulae. In Astrophysical Sources of High Energy Particles and Radiation, ed. B. Rudak, (AIP Conf. Proc. 2005), 801, 298
29. de Jager, O.C., Funk, S. & Hinton, J.A. 2005c, In Proc. of the 29th International Cosmic Ray Conference, 4, 239
30. de Jager, O.C. 2007, ApJ, 658, 1177
31. du Plessis, I., de Jager, O.C. & Buchner, S., et al. , 1995, ApJ, 453, 746
32. Gaensler, B.M., Arons, J., & Kaspi, V.M., et al. , 2002, ApJ, 569, 878
33. Gaensler, B.M., Schulz, N.S., & Kaspi, V.M., et al. , 2003, ApJ, 588, 441
34. Gaensler, B.M. & Slane, P.O. 2006, Ann. Rev. A&A, 44, 17
35. Gallant, Y.A. (for the H.E.S.S. Collaboration), 2007, Ap&SS, 309, 197
36. Gotthelf, E.V. & Olbert, C.M. in Proc. of the 270 WE-Heraeus Seminar on Neutron Stars, Pulsars, and Supernova Remnants, MPE Report 278, Ed. by W. Becker, H. Lesch, & J. Trümper (Garching bei München: Max-Planck-Institut für Extraterrestrische Physik, 2002), 159
37. Gould, R.J. 1965, Phys. Rev. Lett., 15, 577
38. Hales, A.S., Casassus, S., Alvarez, H., et al. , 2004, ApJ, 613, 977
39. Harding, A.K. & Gaisser, T.K. 1990, ApJ, 358, 561
40. Hillas, A.M., et al. (Whipple Collaboration) 1998, ApJ, 503, 744
41. Hinton, J.A., et al. (the H.E.S.S. Collaboration) 2004, New Astron. Rev., 48, 331
42. Hinton, J.A & Aharonian, F.A. 2007, A&A., 657, 302
43. Horns, D., Aharonian, F.A., Santangelo, A., et al. , 2006, A&A, 451, L51
44. Kennel, C.F. & Coroniti, F.V. 1984, ApJ, 283, 710
45. LaMassa, A., Slane, P.O. & de Jager, O.C. 2006, American Astronomical Society Meeting 208, No. 3.03
46. Lemièrre, A., Terrier, R. & Djannati-Ataï, A. 2005, In Proc. of the 29th International Cosmic Ray Conference, 4, 105
47. Lemièrre, A. 2006, Ph.D. thesis, Univ. of Paris 7 and College de France, Paris

48. Milne, D.K. 1995, MNRAS, 277, 1435
49. Mangano, V., Massaro, E., Bocchino, F, et al. , 2005, A&A, 436, 917
50. Markwardt, C.B. & Ögelman, H. 1997, ApJ, 480, L13
51. Matheson, H. & Safi-Harb, S. 2005, Adv. in Space Res., 35, 1099
52. Ng, C.-Y. & Romani, R.W. 2004, ApJ, 601, 479
53. Porquet, D., Decourchelle, A. & Warwick, R.S. 2003, A&A, 401, 197
54. Rees, M.J. & Gunn, J.E. 1974, MNRAS, 167, 1
55. Reynolds, S.P. & Chevalier, R.A. 1984, ApJ, 278, 630
56. Reynolds, S.P. & Chanan, G.A. 1984, ApJ, 281, 673
57. Reynolds, S.P. 1988, ApJ, 327, 853
58. Slane, P.O., Helfand, D., van der Swaluw, E., et al. , 2004, ApJ, 616, 403
59. Sefako, R.R. & de Jager, O.C. 2003, ApJ, 593, 1013
60. Steenberg, C.D. 1988, Ph.D. thesis, North-West University, Potchefstroom Campus
61. van der Swaluw, E. & Wu, Y. 2001, ApJ, 555, L49
62. Wang, Q.D., Li, Z.Y. & Begelman, M.C. 1993, Nature, 364, 127
63. Weiler, K.W. & Panagia, N. 1978, A&A, 70, 419
64. Weiler, K.W. & Panagia, N. 1980, A&A, 90, 269
65. Wilson, D.B. & Rees, M.J. 1978, MNRAS, 185, 297